cmgh
CELLULAR AND MOLECULAR GASTROENTEROLOGY AND HEPATOLOGY

ORIGINAL RESEARCH

Loss of SLC26A3 Results in Colonic Mucosal Immune Dysregulation via Epithelial-Immune Cell Crosstalk

Dulari Jayawardena,[1,§] Shubha Priyamvada,[1] Takahiro Kageyama,[2] Zachary White,[2] Anoop Kumar,[1,3] Theodor F. Griggs,[1] Apurba Majumder,[1] Ramsha Akram,[1] Arivarasu N. Anbazhagan,[1] Teruyuki Sano,[2,§] and Pradeep K. Dudeja[1,3,§]

[1]Department of Medicine, University of Illinois at Chicago, Chicago, Illinois; [2]Department of Microbiology and Immunology, University of Illinois at Chicago, Chicago, Illinois; and [3]Jesse Brown VA Medical Center, Chicago, Illinois

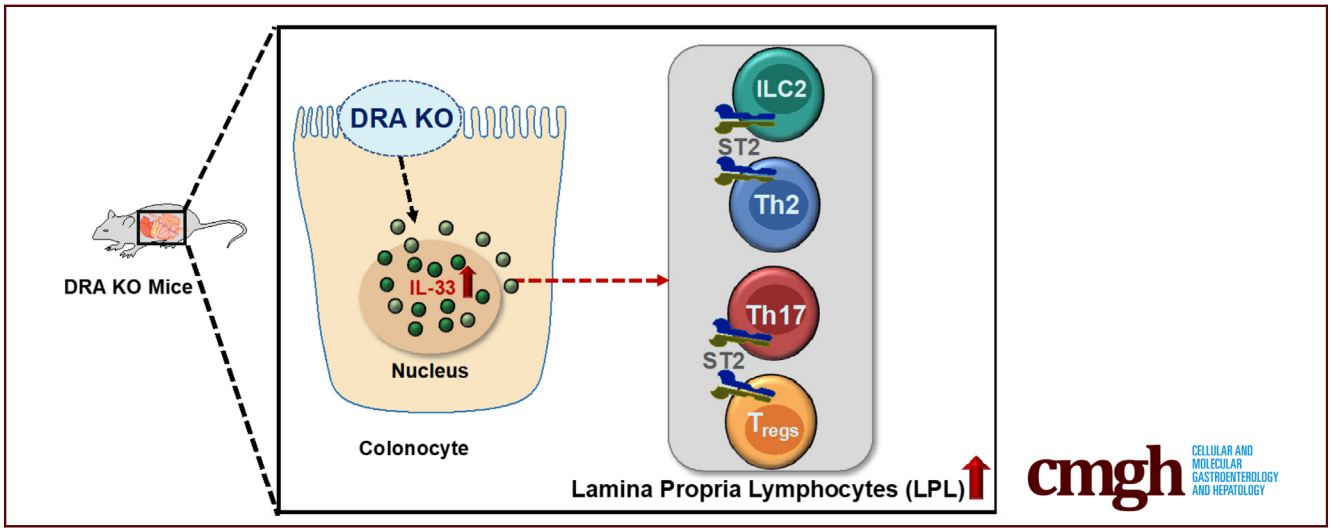

BACKGROUND & AIMS: Down-regulation of chloride transporter SLC26A3 or down-regulated in adenoma (DRA) in colonocytes has recently been linked to the pathogenesis of ulcerative colitis (UC). Because exaggerated immune responses are one of the hallmarks of UC, these current studies were undertaken to define the mechanisms by which loss of DRA relays signals to immune cells to increase susceptibility to inflammation.

METHODS: NanoString Immunology Panel, fluorescence assisted cell sorting, immunoblotting, immunofluorescence, and quantitative real-time polymerase chain reaction assays were used in wild-type and DRA knockout (KO) mice. Interleukin (IL)-33 blocking was used to determine specific changes in immune cells and co-housing/broad spectrum antibiotics administration, and ex vivo studies in colonoids were conducted to rule out the involvement of microbiota. Colonoid-derived monolayers from healthy and UC patient biopsies were analyzed for translatability.

RESULTS: There was a marked induction of Th2 (>2-fold), $CD4^+$ Th2 cells (~8-fold), $ROR\gamma t^+$ Th17, and $FOXP3^+$ regulatory T cells (Tregs). DRA KO colons also exhibited a robust induction of IL-33 (>8-fold). In vivo studies using blocking of IL-33 established that T2 immune dysregulation (alterations in ILC2, Th2, and $GATA3^+$ iTregs) in response to loss of DRA was due to altered epithelial-immune cell crosstalk via IL-33.

CONCLUSIONS: Loss of DRA in colonocytes triggers the release of IL-33 to drive a type 2 immune response. These observations emphasize the critical importance of DRA in mucosal immune homeostasis and its implications in the pathogenesis of UC. *(Cell Mol Gastroenterol Hepatol 2023;15:903–919; https://doi.org/10.1016/j.jcmgh.2022.12.009)*

Keywords: Down Regulated in Adenoma; Type 2 Innate Lymphoid Cells; Regulatory T-cells; Ulcerative Colitis; GATA3; Interleukin-33.

The chloride transporter *SLC26A3* also known as down-regulated in adenoma (DRA) is an intestinal anion exchanger that plays a critical role in electrolyte and water absorption.[1] Recent genome wide association studies have highlighted the emerging role of *SLC26A3* in the pathogenesis of ulcerative colitis (UC).[2–4] In addition, DRA deficiency in mice results in an array of intestinal defects including compromised barrier integrity and microbial dysbiosis, features common to human UC.[5,6] Although at baseline DRA knockout (KO) mice do not show marked inflammation, these mice are more susceptible to intestinal

inflammation, suggesting dysregulation of gut immune homeostasis. In fact, patients with mutations in *SLC26A3* gene display congenital chloride diarrhea (CLD) and have recently been shown to have higher incidence of inflammatory bowel disease (IBD).[7] However, any direct link of loss of DRA to gut immune cell homeostasis and its implications in gut inflammation have not been examined.

Because of the critical importance of DRA in the maintenance of intestinal epithelial integrity and its involvement in UC susceptibility, we speculated that loss of DRA in enterocytes could influence the mucosal immune system via 2 potential mechanisms: (1) indirectly because of the functional deficit of ion transport resulting in alterations in the luminal microenvironment or (2) by directly triggering structural changes in enterocytes to alter the epithelial-immune cell crosstalk. The chloride bicarbonate exchange activity of DRA can have a significant impact on the luminal microenvironment including pH,[6] mucus secretion, and the gut microbiome.[5] Of note, patients with CLD exhibit severe diarrhea, metabolic alkalosis, and acidic stool that is rich in chloride.[8] Therefore, the luminal alterations could have a direct impact on subsequent responses mounted by the mucosal immune system. In this regard, several studies have detailed how alterations in luminal pH during inflammation changes the gut microbiota, thus impacting the immune responses.[9–11] Furthermore, enterocytes serve as a barrier limiting interaction of luminal agents with the immune cells and express cytokines and their cognate receptors, which are important in counterbalancing responses to self-antigens.[12] Epithelial-derived cytokines such as interleukins (ILs) 1, 6, 9, and 33 relay signals to the lamina propria to propagate various immune reactions.[13] We have recently shown that loss of DRA results in compromised barrier integrity by significantly reducing the expression of important tight and adherens junction proteins.[5,14] Therefore, it is likely that changes in the epithelial integrity triggered by loss of DRA could adversely impact secretion of epithelial-derived cytokines and signaling molecules to impact the mucosal immune cell homeostasis.

Alarmin cytokine IL-33, expressed in intestinal epithelial cells (IECs), is a key modulator of T2 immune responses (governed by the master transcription factor GATA3 for Th2 immunity).[15] Numerous studies have shown that IL-33 levels are up-regulated in IECs in IBD patients and in several animal models of colitis.[16–18] Overactivated type 2 immune responses are a hallmark feature of UC.[19] Because dysregulated immune responses govern the underlying pathology in human UC and loss of DRA is a key event observed in colonocytes in UC patients and in animal models of IBD, we hypothesized that loss of DRA will contribute to dysregulation of intestinal lamina propria lymphocytes (LPLs) to increase susceptibility to gut inflammation.

Here we demonstrate that loss of DRA resulted in a significant dysregulation of innate and adaptive lymphocytes. The key findings showed that loss of DRA resulted in (1) robust induction of GATA3$^+$ type 2 innate lymphoid cells (ILC2); (2) reduction in number of RORgt$^+$ type 3 ILCs (ILC3) and IL-22; and (3) marked increase in GATA3$^+$ Th2 as well as RORγt$^+$ Th17 and FOXP3$^+$ natural regulatory T cells (nTregs) underpinning an overactivated mucosal immune system. Furthermore, there was a (4) robust up-regulation of colonocyte IL-33 expression in DRA KO mice compared with their littermate controls (wild-type [WT]). In addition, our co-housing and antibiotic treatment studies of DRA KO mice showed that up-regulation of IL-33 in colonocytes of these mice was predominantly independent of gut microbiota. In addition, studies with a human UC colonoid derived monolayer also demonstrated an increase in IL-33 along with a decrease in DRA expression. Collectively, these data showed that changes in luminal environment and colonocyte alterations in response to loss of DRA trigger release of alarmin molecule IL-33 to drive expansion of type 2 LPLs. These events may contribute to the mechanisms underlying the vital role of deficiency of DRA in UC pathogenesis.

Results

Immune Related Genes Were Markedly Elevated in DRA KO Colonic Mucosa

To understand the differences between colons of WT and DRA KO mice at steady state, we conducted RNA sequencing using the NanoString nCounter immunology panel (Seattle, WA) using colonic mucosa from DRA KO and its littermate controls. After analyzing the data using standard and advanced analysis software, it was observed that colonic tissues of DRA KO mice showed a robust induction of genes linked to cytokines, complement system, and chemokines (Figure 1*A*). Advanced analysis of data using the Nsolver software and the ROSALIND platform showed that the pathway scores for chemokine (Figure 1*B*) and cytokine signaling (Figure 1*C*) were markedly higher in DRA KO colons compared with WT littermates. In addition, heat map represented in Figure 1*D* (created using signature genes to identify and assess the abundance of various innate immune cells) showed that several innate immune cells were significantly elevated in DRA KO mice. These results corroborated the staining data for CD68$^+$ activated macrophages (stained in red), demonstrating accumulation of these cells in DRA KO colons compared with littermate controls (Figure 1*E*). Although innate immune cells showed an increase, the prominent gene signature identified in the NanoString data was an enhancement of type 2 immune tone shown in the heat map (Figure 1*F*) where several genes important for type 2 immunity were up-regulated in DRA KO colons. Likewise, pathway analysis further showed that

§Authors share co-senior authorship.

Abbreviations used in this paper: CLD, congenital chloride diarrhea; DRA, down-regulated in adenoma; DSS, dextran sulfate sodium; IBD, inflammatory bowel disease; IEC, intestinal epithelial cell; ILC, innate lymphoid cell; KO, knockout; LPL, lamina propria lymphocyte; Treg, regulatory T cell; T2, type 2; UC, ulcerative colitis; WT, wild-type.

Most current article

2352-345X
https://doi.org/10.1016/j.jcmgh.2022.12.009

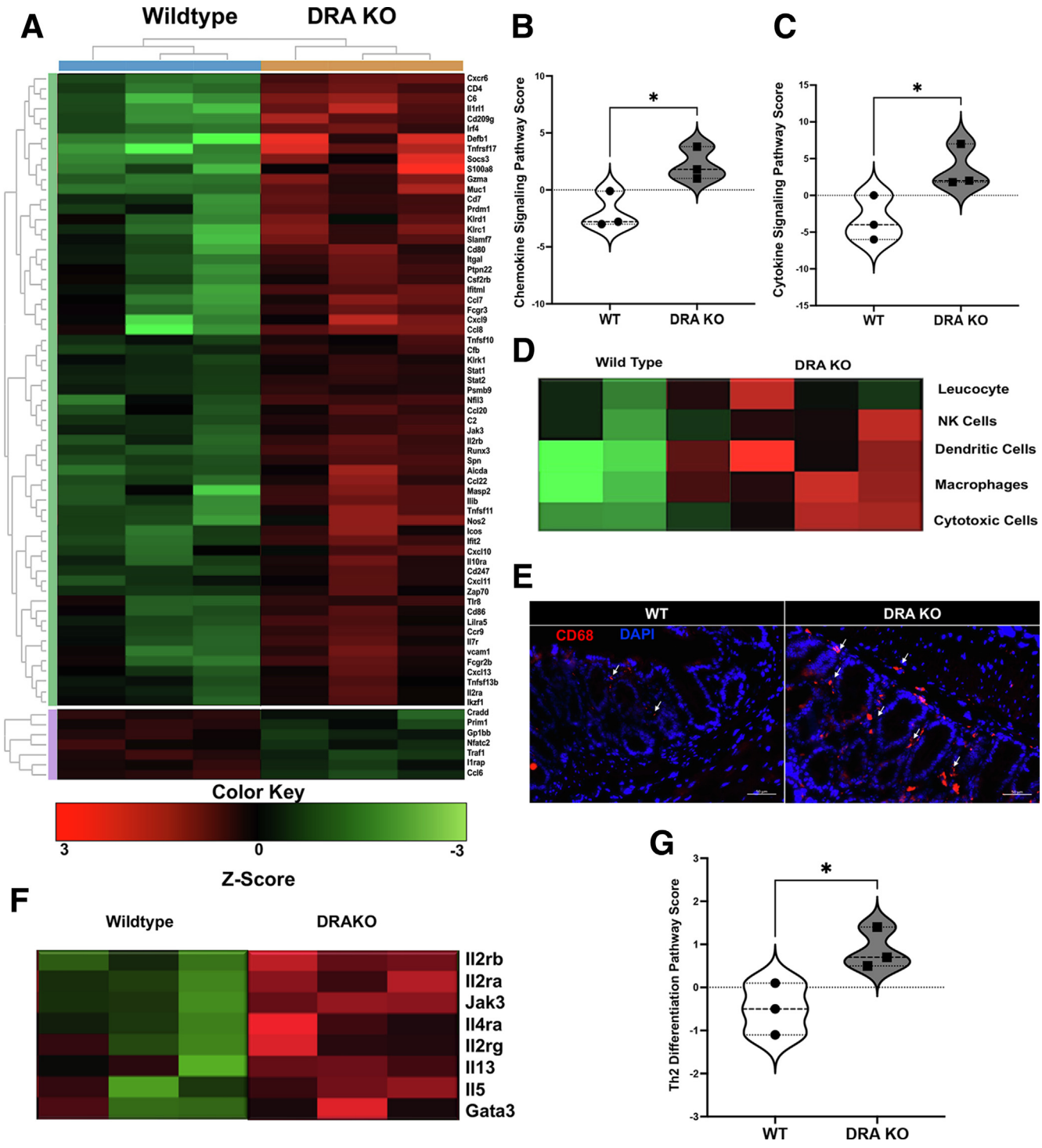

Figure 1. DRA KO mice colonic mucosa showed an overactivated immune cell signature. WT and DRA KO (n = 3) distal colonic mucosal RNA was subjected to NanoString nCounter Immunology Panel. (*A*) Heat map demonstrates significantly up-regulated (*red*) immune related genes in WT and DRA KO mice. Representative violin plot for pathway scores contains (*B*) chemokine signaling and (*C*) cytokine signaling. (*D*) Heat map demonstrates differential expression of various innate immune cells based on genes previously shown to be characteristic of various cell populations. (*E*) CD68 (*red*) staining in cryosections of WT and DRA KO mice distal colonic mucosa, scale bar 50 μm. (*F*) Heat map shows highly up-regulated genes of type 2 immune pathways. (*G*) Pathway scores based on genes related to Th2 differentiation. All pathway score analysis was conducted using nSolver software advanced analysis and ROSALIND software. Data presented as mean ± standard error of mean, n = 3. *$P < .05$ vs WT.

Th2 differentiation score was also significantly increased in DRA KO colons (Figure 1*G*). Several other differentiation scores for adaptive effector T cells (Th17 and Tregs) also showed a trend toward an increase in DRA KO colonic tissues (data not shown). Therefore, we next aimed at quantifying various LPLs in WT vs DRA KO colonic tissues to confirm our NanoString data.

DRA KO Mice Showed Significantly Altered Colonic Lamina Propria Innate Lymphoid Cells

Because majority of the defects observed in DRA KO mice were most prominent in the colon, we sought to determine amounts of total CD127$^+$ ILCs and the different subtypes present in the colonic LP by flow cytometric analysis (Figure 2*A*). Compared with WT littermates, the total ILC numbers were significantly up-regulated in DRA KO mice colons (Figure 2*B*). The increase in total ILC numbers was parallel to the robust induction of the GATA3$^+$ ILC2 (Figure 2*C*–*E*) in DRA KO mice colons with no effect on ILC1 (data not shown). There was a 2-fold induction of ILC2s in DRA KO compared with WT at baseline. It has been recently shown how the intestinal epithelium can contribute to changes in the ILC populations via IL-25 and tuft cells.[20] To elucidate whether a similar mechanism was involved in the up-regulation of ILC2s in the colon, we first determined the mRNA expression of IL-25 and observed a significant up-regulation in DRA KO colonic mucosa (Figure 2*F*). Similarly, we determined whether there was an increase in tuft cell numbers in the colonic epithelium. As depicted in Figure 2*G* and *H*, the numbers of tuft cells identified by DCLK1$^+$ cells (green) were similar in both WT and DRA KO mice colons parallel to unchanged mRNA levels (data not shown). These data indicated that tuft cell hyperplasia can be ruled out as a potential contributor to increased ILC2s in colonic LP. In addition to staining for tuft cells, we also examined any potential changes in DCLK1 protein isoforms (short and long). Interestingly, the long form of DCLK1 was significantly lower in DRA KO mice, with a concomitant increase in the short form of DCLK1 that was similar to what is observed in colonic cancers (Figure 2*I*–*K*). In addition, we also quantified the number of periodic acid-Schiff positive goblet cells and found no significant change in DRA KO mice (data not shown).

We next examined the levels of RORγt$^+$ type 3 ILCs (ILC3) by fluorescence-activated cell sorting, which are known to play an important role in affecting barrier integrity and maintaining homeostasis in the intestinal epithelium. There was a substantial drop in the total number of ILC3s in the colonic LP (Figure 2*L* and *M*). These beneficial effects of ILC3s have mainly been attributed to the secreted cytokine IL-22. In this regard, our data showed that the subtype of ILC3 expressing NKp46 (important for IL-22 secretion) was severely reduced in the DRA KO mice colons (Figure 2*N*). Consistent with these findings, the important cytokine secreted by NKP46$^+$ ILC3 was also considerably decreased in DRA KO mice colons as depicted in Figure 2*O*. Parallel to the data in colonic LP, DRA KO mice ileal lamina propria also exhibited significantly lower levels of total ILCs and the subtype ILC3 (Figure 2*P*–*R*) with no changes in ILC2s (data not shown).

Effector T-Cell Populations in the Colonic Lamina Propria of DRA KO Mice Exhibited a Type 2 Phenotype

We next determined the levels of effector CD4$^+$ T-cell populations in ileal LP, colonic LP, and mesenteric lymph nodes in WT and DRA KO mice. Intriguingly, as opposed to what was observed in the ILC populations, there were no significant differences in the total CD4$^+$ T-cell numbers as well as various subpopulations including the Th1, Th2, Th17, and Tregs in the ileum and the mesenteric lymph nodes (data not shown). In contrast to the ileum, there were significant differences in various T-cell populations (gating strategy in Figure 3*A*) in the colon. Although the total number of T cells remained unchanged in the colon of DRA KO mice compared with WT, there was a significant up-regulation of all CD4$^+$ T cells except Tbet$^+$ Th1 cells (data not shown). In contrast, GATA3$^+$ CD4$^+$ T cells were markedly increased in the colonic LP of DRA KO mice compared with WT littermates (Figure 3*B*–*E*). Next, we examined the expression of RORγt and FOXP3 in these cells to distinguish Th17 (Foxp3$^-$ RORγt$^+$ cells), natural Tregs (Foxp3$^+$ RORγt$^-$ cells), and inducible Tregs (iTregs) (Foxp3$^+$ RORγt$^+$) (Figure 3*F*–*M*). A robust induction of all 3 subsets of T-helper cells was observed in the colonic LP of DRA KO mice (Figure 3*F*–*M*). Finally, another type of inducible Treg (GATA3$^+$ and FOXP3$^+$) were also more than doubled in the colonic LP of DRA KO mice, indicating an induction of these cells as well (Figure 3*N*–*P*). However, the GATA3$^+$ and RORγt$^+$ iTregs in the ileal LP remained unaltered in DRA KO mice (data not shown). Interestingly, GATA3$^+$ iTregs are predominantly accumulated at mucosal surfaces and are known to be heavily dependent on IL-33.[21]

DRA KO Colonocytes Harbor Markedly High Levels of the Alarmin IL-33 and This Increase Was Predominantly Independent of the Gut Microbiota

We next examined the roles of epithelial derived factors that could bolster both type 2 immune cell populations. Hence, we analyzed the levels of the alarmin IL-33 in DRA KO mice colonic mucosa. Although IL-33 mRNA levels were unchanged (data not shown), the protein levels were significantly up-regulated (Figure 4*A* and *B*) in DRA KO colons (>8-fold), with no changes in its receptor *IL1RL1* or ST2 protein expression (data not shown). This cytokine was identified to be the epithelial IL-33, which was localized to the nucleus, as is clearly depicted in Figure 4*C*. In parallel to changes in IL-33, the type 2 effector protein amphiregulin was also significantly elevated (>3-fold) in DRA KO mice colons, confirming the functional relevance of an up-regulated type 2 immune tone in DRA KO mice (Figure 4*D* and *E*). Furthermore, IL-33 was released mainly from colonic explants of DRA KO mice and very minimally from ileal explants of DRA KO mice compared with WT mice (Figure 4*F*), with no change in serum IL-33 levels (data not shown). Next, we further investigated whether the up-regulation of IL-33 was dependent on gut microbiota; we treated DRA KO mice with broad spectrum antibiotics

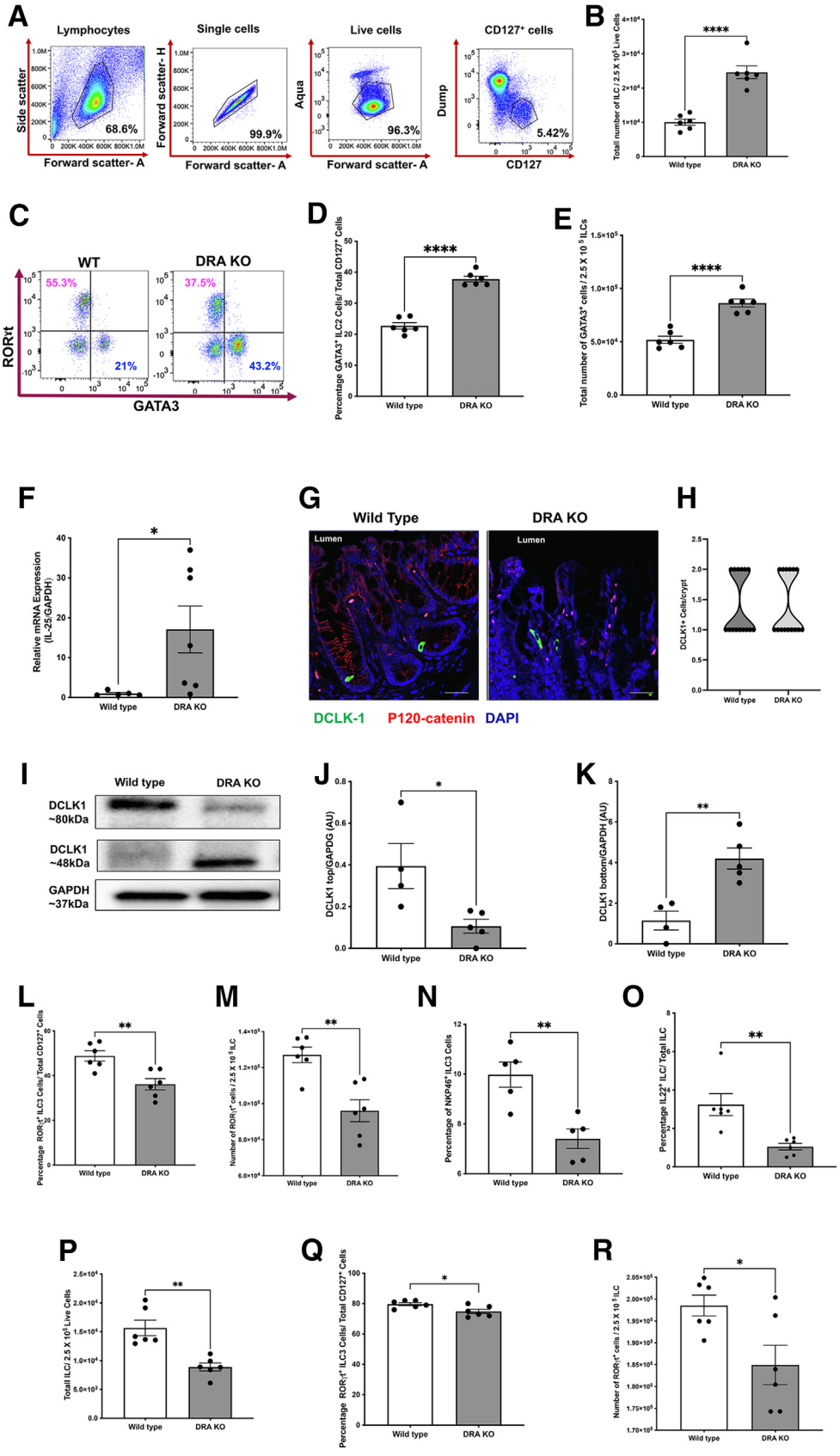
A
Lymphocytes
Single cells
Live cells
CD127+ cells
Side scatter
Forward scatter- A
Forward scatter- H
Aqua
Dump
CD127
68.6%
99.9%
96.3%
5.42%
B
****
Totall number of ILC / 2.5 X 10^5 Live Cells
Wild type
DRA KO
C
WT
DRA KO
55.3%
21%
37.5%
43.2%
RORγt
GATA3
D
****
Percentage GATA3+ ILC2 Cells/ Total CD127+ Cells
E
****
Total number of GATA3+ cells / 2.5 X 10^5 ILCs
F
*
Relative mRNA Expression (IL-25/GAPDH)
G
Wild Type
DRA KO
Lumen
DCLK-1
P120-catenin
DAPI
H
DCLK1+ Cells/crypt
I
Wild type
DRA KO
DCLK1 ~80kDa
DCLK1 ~48kDa
GAPDH ~37kDa
J
*
DCLK1 top/GAPDG (AU)
K
**
DCLK1 bottom/GAPDH (AU)
L
**
Percentage RORγt+ ILC3 Cells/ Total CD127+ Cells
M
**
Number of RORγt+ cells / 2.5 X 10^5 ILC
N
**
Percentage of NKP46+ ILC3 Cells
O
**
Percentage IL22+ ILC/ Total ILC
P
**
Totall ILC/ 2.5 X 10^5 Live Cells
Q
*
Percentage RORγt+ ILC3 Cells/ Total CD127+ Cells
R
*
Number of RORγt+ cells / 2.5 X 10^5 ILC

containing water or regular water for 7 days. However, IL-33 and amphiregulin (data not shown) still remained increased in antibiotics treated DRA KO mice (Figure 4*G* and *H*). For ruling out the effect of altered gut microbiome observed in DRA KO mice impacting IL-33 secretion, the co-housing studies were also carried out.[5] Consistent with the results of antibiotic treatment, our results showed that IL-33 levels were still elevated in co-housed DRA KO mice and were not increased in WT mice co-housed with DRA KO mice (Figure 4*I* and *J*). In addition, in colonoids prepared from WT and DRA KO mice, it was also observed that IL-33 was increased only in DRA KO colonoids (Figure 4*K*–*M*).

Neutralization of IL-33 in DRA KO Mice Alleviated the Type 2 Immune Cell Phenotype in Colonic Lamina Propria

Elevated colonic IL-33 in DRA KO mice appeared to be the most prominent driving factor in skewing the colonic LP lymphocytes to a type 2 subtype. Therefore, to confirm this observation, we administered IL-33 neutralizing antibody to DRA KO mice via intraperitoneal injection for 1 week to determine whether these effects could be reversed. In fact, weekly administration of anti-IL-33 antibody to DRA KO mice resulted in a significant reduction in type 2 immune cells including ILC2s (Figure 5*A*–*C*), Th2 (Figure 5*D* and *E*), and the GATA3$^+$ iTregs (Figure 5*F* and *G*) with no changes in ILC3s and Tregs (data not shown), validating that IL-33 is the cytokine mainly responsible for triggering this type 2 immune cell expansion in the colonic LP of DRA KO mice.

Dextran Sulfate Sodium Challenge Further Exacerbated Immune Cell Changes in DRA KO Mice

Dextran sulfate sodium (DSS) model has been shown to potentiate type 2 immune cells via induction of IL-33.[22,23] Thus, it was of interest to investigate how DSS acute injury model could modulate the various immune cell populations in the LP of DRA KO mice. Interestingly, the changes observed at baseline in DRA KO mice were further exaggerated with DSS treatment (Figure 6). The specific changes included increased ILC2 levels (Figure 6*A*) and reduced ILC3 levels (Figure 6*B*) in the innate lymphocytic compartment. In parallel, GATA3$^+$ cells were expanded with DSS insult in WT mice, which was similar to what was observed in DRA KO mice at baseline. However, these changes were further enhanced with DSS challenge in DRA KO mice colonic LP (Figure 6*C*). Th17 and nTregs were all elevated in DRA KO colonic LP including the specific subpopulations of inducible Tregs/iTregs (Figure 6*D*–*G*). Both IL-22 and IL-17 showed an increase in DRA KO colonic LP, demonstrating an overactivation of RORγt$^+$ cell populations in the adaptive immune compartment in DSS colitis (Figure 6*H* and *I*). Interestingly, the DSS challenge in DRA KO mice did not further induce IL-33 protein levels (Figure 6*J* and *K*). Collectively, these data indicate that DRA KO mice mimic some of the changes observed in DSS colitis mouse model, which is a widely used model for human UC, and that under DSS challenge the effects observed at baseline are amplified.

Colonocytes of a Patient With Human Ulcerative Colitis Exhibited Up-regulated IL-33 Along With Lower Levels of DRA

Because IL-33 is also increased in the inflamed human intestine, specifically in human UC,[24] to validate these findings, colonoid-derived monolayers were prepared from a healthy control and a patient diagnosed with severe UC and were stained for IL-33. Interestingly, there was a strong augmentation of IL-33 protein (green) in the colonocytes of UC patient-derived colonic monolayers compared with healthy control (Figure 7*A*). Furthermore, as established before,[25,26] we observed that DRA expression (green) was markedly repressed in UC colonoid-derived monolayers (Figure 7*B*). Although these data are derived only from a single patient sample, because we and others have previously shown that DRA is markedly reduced in colitis[25–27] and IL-33 is also increased in colitis,[16,24] these data further confirm this potential direct relationship in human situation as well. Next, to ascertain whether a similar phenomenon is observed in DRA KO mice, colonoid-derived monolayers from WT and DRA KO mice were prepared and stained for IL-33 (green). As depicted in Figure 7*C*, DRA KO colonoid-derived monolayers showed a marked

Figure 2. (***See previous page***). **Innate lymphoid cell populations in colonic and ileal lamina propria of DRA KO mice were dysregulated.** Isolated colonic lamina propria lymphocytes were gated for CD127$^+$ innate lymphoid cells (ILCs), followed by various subtypes using fluorescence assisted cell sorting (FACS). (*A*) Gating strategy used for ILCs (Dump: CD3e, CD11b, CD14, CD19, B220, TCR$\gamma\delta$). (*B*) Bar diagram shows total number of ILCs in colonic lamina propria of WT vs DRA KO mice. (*C*) Representative dot plot depicts number of GATA3$^+$ ILCs (lower right quadrant, labeled in *blue*) and ILC3s (upper left quadrant labeled in *magenta*) in WT vs DRA KO mice. Bar graph shows (*D*) percentage and (*E*) total number of ILC2s in colonic lamina propria of WT vs DRA KO mice. (*F*) Bar graph represents relative mRNA expression of interleukin-25 (IL-25) in WT and DRA KO mice. (*G*) Representative images of DCLK1 (*green*), P-120 catenin (*red*) stained distal colonic cryosections of WT vs DRA KO mice, scale bar 20 μm. (*H*) Representative truncated violin plot shows number of DCLK1$^+$ tuft cells per crypt of WT and DRA KO mice. (*I*) Representative Western blot shows bands for high molecular weight/long form of DCLK1 (Doublecortin like kinase-1) (~80 kDa) and low molecular weight/short form (~48 kDa) isoforms and GAPDH in WT vs DRA KO mice. (*J*) Densitometric analysis of high molecular weight (long form) and (*K*) low molecular weight (short form) isoform of DCLK1 normalized to GAPDH. Bar diagram for (*L*) percentage and (*M*) total number of RORγt$^+$ ILC3s in colonic lamina propria. Bar graph depicts (*N*) percentage of NKP46$^+$ ILC3s and (*O*) IL-22$^+$ ILC3s in WT vs DRA KO mice. (*P*) Bar graph shows total number of ILCs/total lamina propria lymphocytes in ileum of WT vs DRA KO mice. Bar graph shows (*Q*) percentage and (*R*) total number of RORγt positive ILC3s per total ILCs in WT vs DRA KO mice ileal lamina propria. Data are presented as mean ± standard error of mean, n = 4–7. *$P < .05$, **$P < .005$, ****$P < .0001$ vs WT.

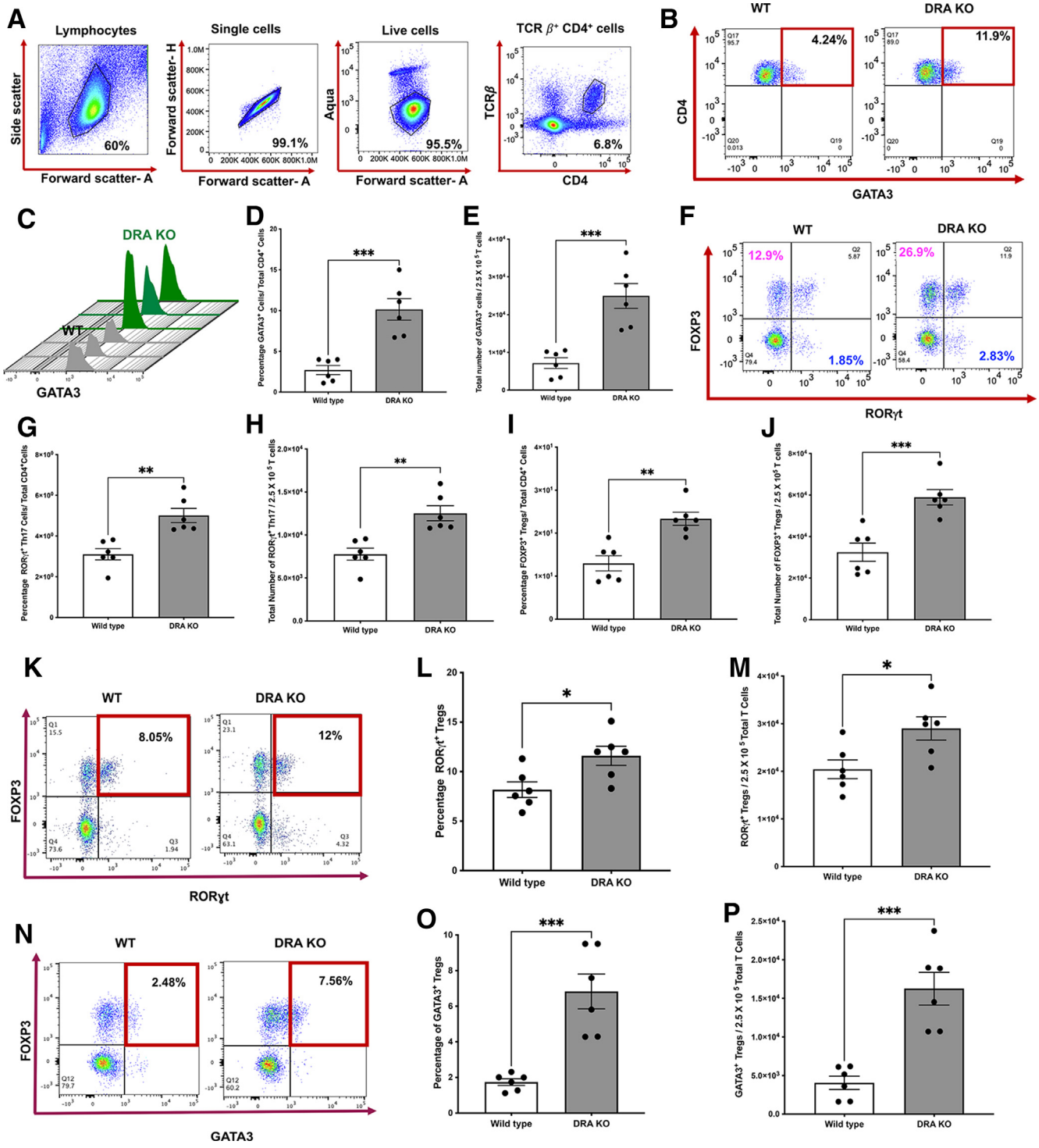

Figure 3. Effector T cells of DRA KO mice colonic lamina propria exhibited a type 2 phenotype. Isolated colonic lamina propria lymphocytes were gated for $CD4^+$ and $TCR\beta^+$ effector T cells (Th), followed by various subtypes using fluorescence assisted cell sorting (FACS). (*A*) Gating strategy used for $CD4^+$ T cells. (*B*) Dot plot shows $CD4^+$ and $GATA3^+$ double positive Th2 in WT vs DRA KO mice. (*C*) Histogram show 3 peaks for GATA3 in WT (*black*) and DRA KO mice (*green*). Bar diagram shows (*D*) percentage and (*E*) total number of $GATA3^+$ effector T cells in WT and DRA KO mice. (*F*) Representative dot plot shows $ROR\gamma t^+$ Th17 (lower right quadrant, labeled in *blue*) and $FOXP3^+$ Tregs (upper left quadrant, labeled in *magenta*) in WT and DRA KO mice. Bar graph shows (*G*) percentage and (*H*) total number of $ROR\gamma t^+$ Th17 cells. Bar diagram represents (*I*) percentage and (*J*) total number of $FOXP3^+$ Tregs in WT and DRA KO mice. (*K*) Representative dot plot shows $ROR\gamma t^+$ and $FOXP3^+$ populations. Bar diagram shows (*L*) percentage and (*M*) total number of $ROR\gamma t^+$ and $FOXP3^+$ iTregs in WT vs DRA KO mice. (*N*) Representative dot plot for $FOXP3^+$ and $GATA3^+$ iTregs. Bar diagram shows (*O*) percentage and (*P*) total number of $GATA3^+$ and $FOXP3^+$ iTregs. Data are presented as mean ± standard error of mean, n = 6–7. $^*P < .05$, $^{**}P < .005$, $^{***}P < .0005$ vs WT.

up-regulation of nuclear IL-33, which disseminated to the cytoplasmic compartment.

Discussion

The chloride bicarbonate exchanger *SLC26A3* or DRA has recently emerged as an important gene involved in the pathogenesis of UC.[1] Furthermore, several studies including our previous work using DRA KO mice have elucidated the diverse roles of DRA apart from its electrolyte absorption and ion transport function.[5,6,28] The current studies establish a novel facet of the role of DRA deficiency in mucosal immune dysregulation via aberrant epithelial-immune cell crosstalk.

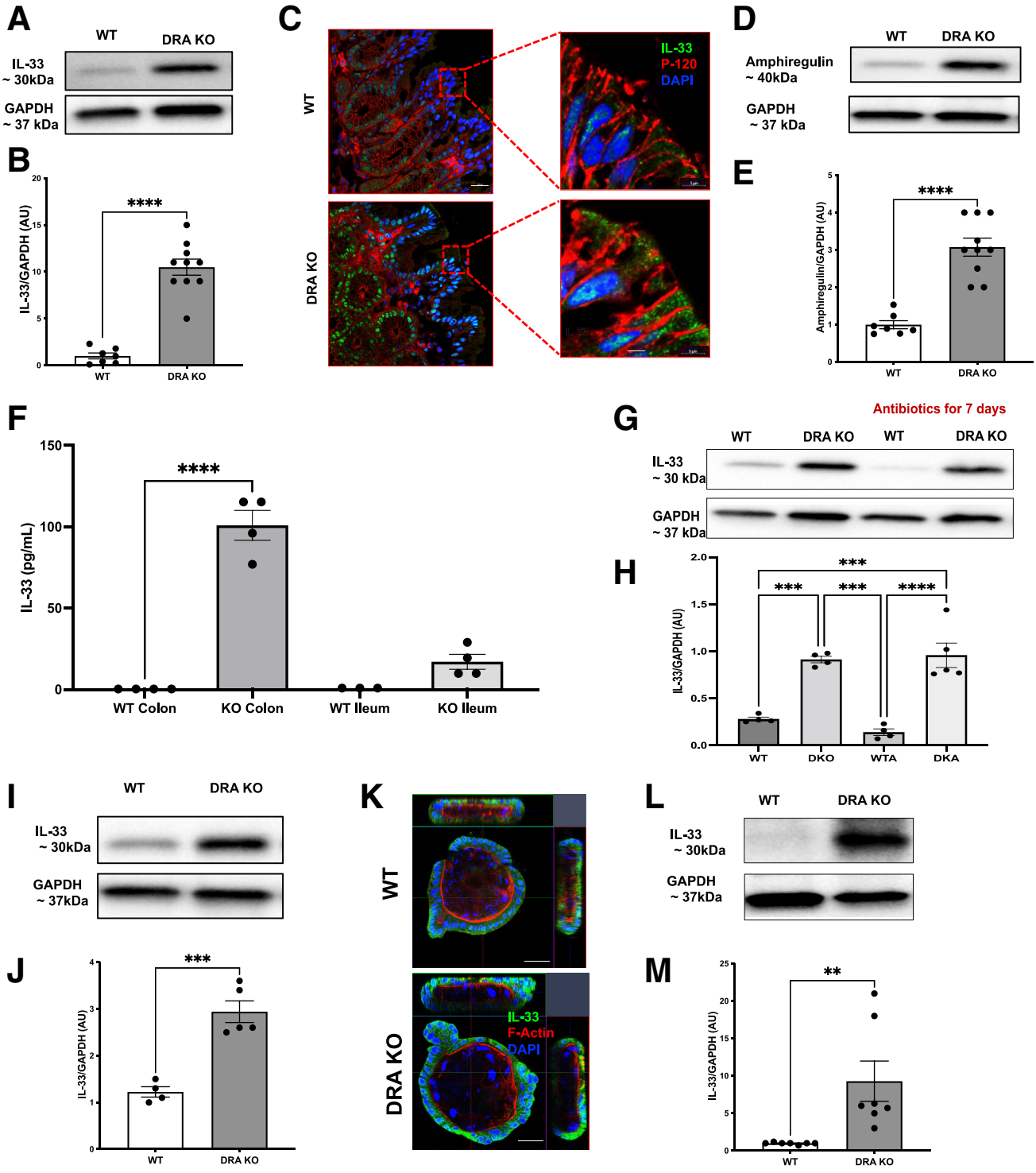

Here, we demonstrate how the loss of DRA can increase epithelial secreted alarmin cytokine IL-33 to enrich the LPLs with type 2 lymphocytes, Th17, and Tregs. In addition, we showed clinical relevance of our data by presenting a similar reduction in DRA with concomitant increase in IL-33 staining in human colonocytes derived from a UC patient.

Although our studies were mainly focused on lymphocytes, the role of antigen presenting cells that also express the IL-33 receptor ST2 cannot be negated. In fact, we observed that levels of activated macrophages were also higher in the colonic mucosa of DRA KO mice. A previous study has also shown similar observations where mRNA expression of immune cell markers including *Cd3e*, *Ly6g*, IL-13, as well as protein expression of Lipocalin-2 was shown to be elevated in the colons of DRA KO mice.[6] Therefore, macrophages could also partake in disseminating signals to the lymphocytic compartment for enrichment of type 2 lymphocytes. Although studies have shown that epithelial ST2 levels are altered during active colitis in patients,[16] we did not observe changes in ST2 protein expression in DRA KO colonic mucosa.

The ILCs are largely resident of the native intestine.[29] During inflammatory states such as IBD, the relative levels of ILC1 and 2 increase at the expense of ILC3s because of high cellular plasticity observed in these cell populations.[30] ILC3 is known to be crucial in maintaining self-tolerance via eradicating the body of self-antigen raised T cells.[31,32] The enrichment of ILC2s, specifically in the colonic LP, was a prominent feature in DRA KO mice. In this regard, a widely established epithelial-immune cell crosstalk pathway is the tuft cell–IL-25–ILC2 circuit.[20,33] Specifically, during helminthic infection the intestinal chemosensory tuft cells secrete IL-25 cytokine to activate ILC2s, which in turn secrete IL-13 and cause tuft cell and goblet cell hyperplasia as a compensatory mechanism to expel the parasites from the intestine.[34] Although this phenomenon has been widely studied in the small intestine, in our current study it was pursued as a potential mechanism in the DRA KO colons. Although we detected an increase in IL-25 and IL-13 mRNA in DRA KO colons, tuft cell hyperplasia was absent. However, the differential expression of 2 isoforms of DCLK1 was detected in DRA KO colons. In addition, both WT and DRA KO mice were screened for the absence of the parasite *Tritrichomonas muris* to ensure that the immune changes were not due to the presence of any parasite (data not shown). Intriguingly, IL-33 up-regulation and the expansion of GATA3$^+$ Tregs have also been observed in colonic cancers, which was a striking feature observed in DRA KO colons.[35,36] Because DRA was initially identified as a protein significantly reduced in adenomas and cancers, this aspect of the role of DRA in colonic carcinogenesis warrants further investigation.

One of the interesting observations of this study was a robust induction of all Treg subpopulations in DRA KO colons. Notably, the FOXP3$^+$ RORγt$^+$ iTreg expansion governed by intestinal microbiota plays a significant role in immune homeostasis and defense at mucosal surfaces specifically in the gut.[37] Recent studies have also highlighted how lack of this subset of Tregs could exacerbate IBD.[38] Alternatively, the FOXP3$^+$ GATA3$^+$ iTregs also play a key role in the intestine and ablation of GATA3; specifically in Tregs have been shown to result in severe inflammation at mucosal sites, indicating its specialized function in maintaining mucosal defense and homeostasis.[21] The luminal changes observed in DRA KO mice, specifically in relation to microbiota, could potentially affect certain immune cell populations (Th17 and RORγt$^+$ iTregs). Although IL-33 up-regulation in DRA KO mice seemed to be predominantly independent of microbiota, in future studies it would be of interest to elucidate which specific immune cells could be driven by the pathogenic bacteria enriched in DRA KO colons. Collectively, the expansion of Tregs indicates that the severe effects caused by loss of DRA may have activated these cells as a compensatory mechanism.

Although multiple studies have established that IL-33 is up-regulated in human IBD, its precise role in its pathogenesis remains elusive.[39] Our current study shows parallel findings to a very recent study in relation to IL-33 in DSS-induced colitis, showing a robust expansion of ILC2s and Tregs. However, in the context of DRA knock-down and a compromised barrier function, DSS colitis further exacerbated the increased type 2 as well as Th17 and Tregs in these mice. Because Th17 and related cytokines were also overactivated in the colon of DRA KO mice challenged with DSS, these data further emphasize the key role of IL-33 in colitis. Although our studies show strong indication that the expansion of these immune cells is driven by IL-33, it does not show a direct link between loss of DRA and up-

Figure 4. (***See previous page***). **The alarmin cytokine interleukin-33 is robustly elevated in DRA KO colons, and this increase was independent of gut microbiota.** (*A*) Representative Western blot and (*B*) bar diagram of densitometric analysis of IL-33 protein expression normalized to glyceraldehyde 2,3 dehydrogenase (GAPDH) in WT and DRA KO mice distal colonic mucosa. (*C*) Representative immunofluorescence image of IL-33 (*green*) and P-120 catenin (*red*) stained in distal colonic frozen sections (5-μm thickness), scale bars 20 μm and 5 μm (inset). (*D*) Representative Western blot and (*E*) bar diagram of densitometric analysis of amphiregulin normalized to GAPDH in WT vs DRA KO mice distal colonic mucosa. (*F*) Representative bar graph shows IL-33 levels in WT and DRA KO mice explant supernatants at 16 hours using the IL-33 enzyme-linked immunosorbent assay (R & D Biosystems). (*G*) Representative Western blot and (*H*) bar diagram of densitometric analysis of IL-33 protein expression normalized to GAPDH after 1 week of oral broad spectrum antibiotic treatment (ampicillin [1 g/L], vancomycin [500 mg/L], neomycin sulfate [1 g/L], and metronidazole [1 g/L]) in WT vs DRA KO mice (DKA, DRA KO mice receiving antibiotics; WT, wild-type; WTA, WT mice receiving antibiotics). (*I*) Representative Western blot and (*J*) bar diagram of densitometric analysis of IL-33 protein expression normalized to GAPDH in WT and DRA KO mice co-housed for over 4 weeks.[5] (*K*) Representative confocal Z-stack images of colonoids stained with IL-33 (*green*) and F-actin (*red*) in WT and DRA KO mice, scale bar 5 μm. (*L*) Representative Western blot and (*M*) bar diagram of densitometric analysis of IL-33 protein expression normalized to GAPDH in WT and DRA KO mice colonoids. Data are presented as mean ± standard error of mean, n = 4–8. $^{**}P < .005$, $^{***}P < .0005$, $^{****}P < .0001$ vs WT.

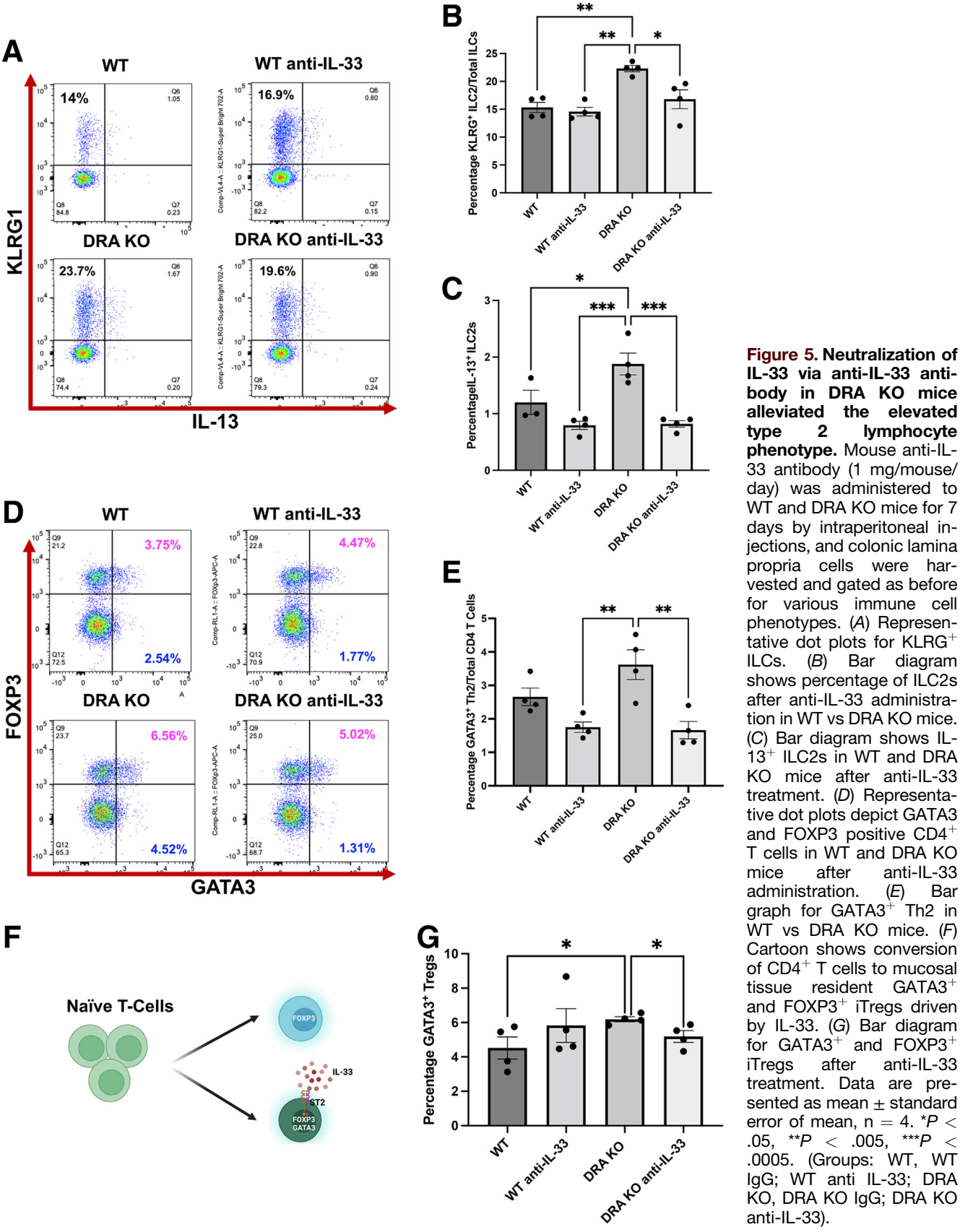

Figure 5. Neutralization of IL-33 via anti-IL-33 antibody in DRA KO mice alleviated the elevated type 2 lymphocyte phenotype. Mouse anti-IL-33 antibody (1 mg/mouse/day) was administered to WT and DRA KO mice for 7 days by intraperitoneal injections, and colonic lamina propria cells were harvested and gated as before for various immune cell phenotypes. (*A*) Representative dot plots for KLRG$^+$ ILCs. (*B*) Bar diagram shows percentage of ILC2s after anti-IL-33 administration in WT vs DRA KO mice. (*C*) Bar diagram shows IL-13$^+$ ILC2s in WT and DRA KO mice after anti-IL-33 treatment. (*D*) Representative dot plots depict GATA3 and FOXP3 positive CD4$^+$ T cells in WT and DRA KO mice after anti-IL-33 administration. (*E*) Bar graph for GATA3$^+$ Th2 in WT vs DRA KO mice. (*F*) Cartoon shows conversion of CD4$^+$ T cells to mucosal tissue resident GATA3$^+$ and FOXP3$^+$ iTregs driven by IL-33. (*G*) Bar diagram for GATA3$^+$ and FOXP3$^+$ iTregs after anti-IL-33 treatment. Data are presented as mean ± standard error of mean, n = 4. *P < .05, **P < .005, ***P < .0005. (Groups: WT, WT IgG; WT anti IL-33; DRA KO, DRA KO IgG; DRA KO anti-IL-33).

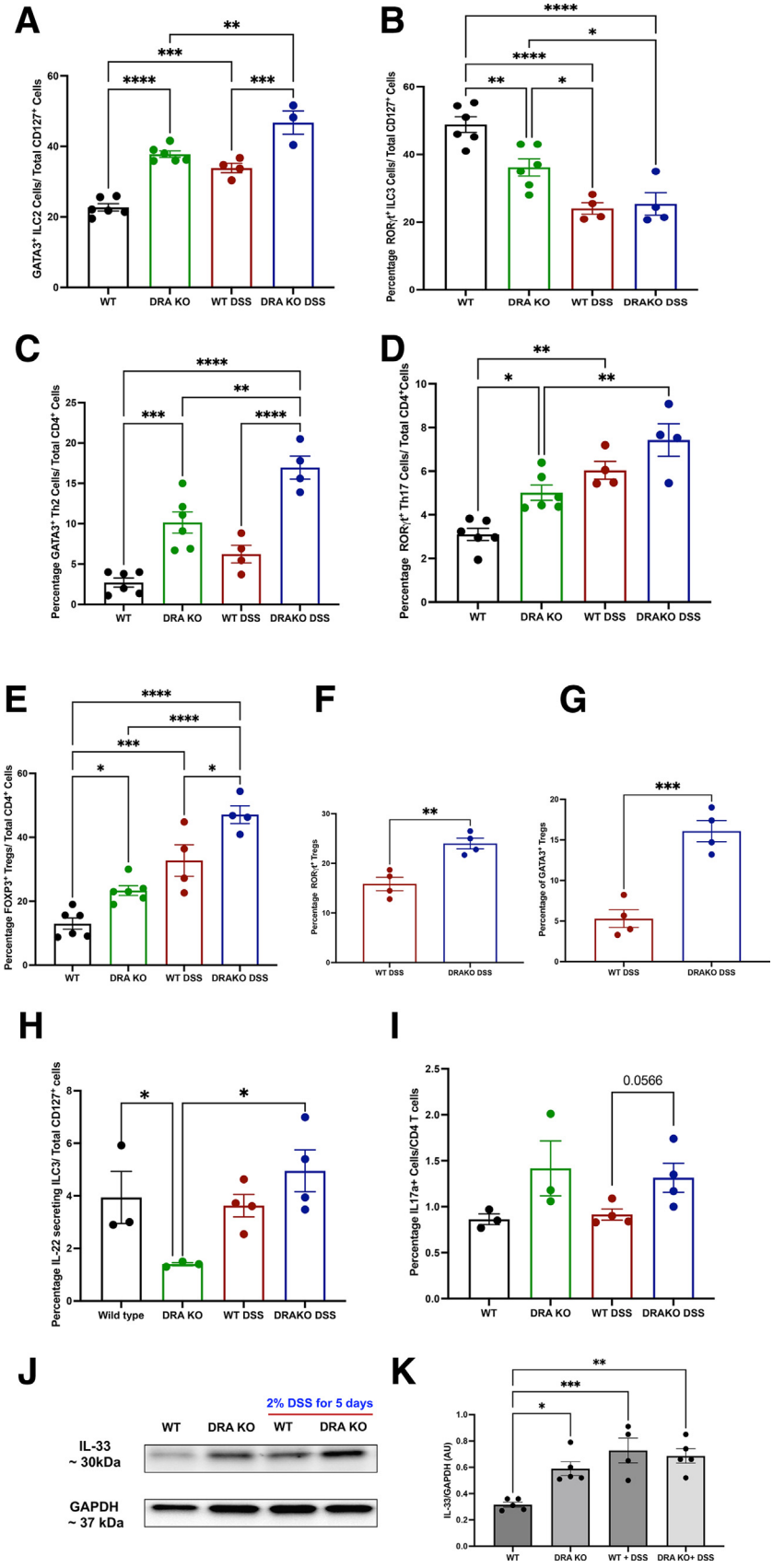

Figure 6. Dextran sulfate sodium induced colitis exaggerates baseline lymphocytic changes in DRA KO mice. WT and DRA KO mice were subjected to 2% dextran sulfate sodium (DSS) in drinking water for 5 days. (*A*) Bar graphs show percentages of $CD127^+$ $GATA3^+$ ILC2s and (*B*) $CD127^+$ and $ROR\gamma t^+$ ILC3s. (*C*) Bar graphs show percentages of $CD4^+$ $GATA3^+$ Th2, (*D*) $ROR\gamma t^+$ Th17, (*E*) $FOXP3^+$ Tregs, (*F*) $ROR\gamma t^+$ and $FOXP3^+$ iTregs, (*G*) $GATA3^+$ and $FOXP3^+$ iTregs, (*H*) IL-22^+ ILCs, and (*I*) IL$17a^+$ $CD4^+$ T cells; *P* value shown above bar graph. (*J*) Representative Western blot and (*K*) densitometric analysis of colonic IL-33 protein levels in WT and DRA KO mice subjected to DSS insult. Groups: WT; DRA KO, drinking water only; WT DSS; DRA KO DSS, mice receiving 2% DSS in drinking water. Data are presented as mean ± standard error of mean, n = 3–6. $^*P < .05$, $^{**}P < .005$, $^{***}P < .0005$, $^{****}P < .0001$ vs WT.

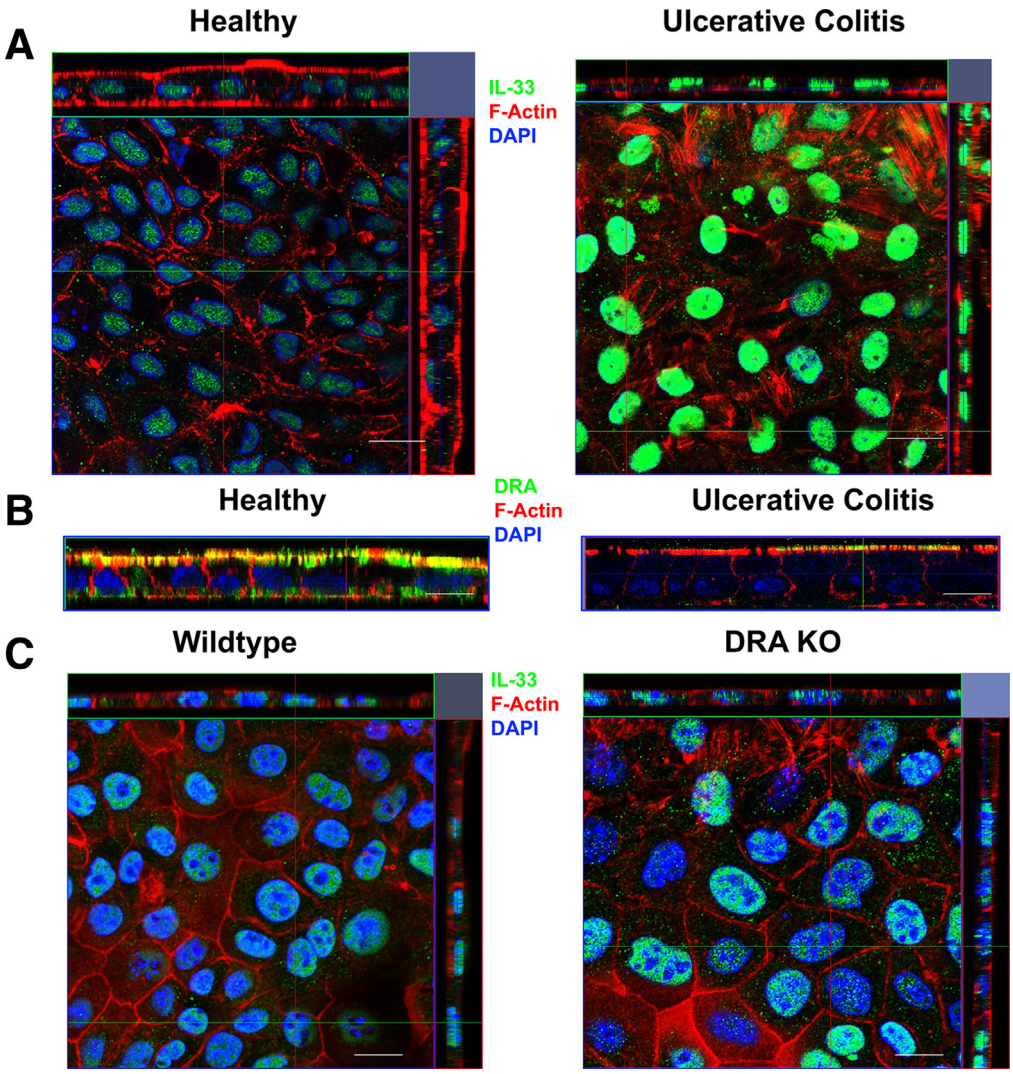

Figure 7. Colonocytes of a patient with human ulcerative colitis exhibited up-regulated IL-33 along with lower levels of DRA. (*A*) Representative Z-stack confocal images of colonoid-derived monolayers stained with IL-33 (*green*) and F-actin (*red*) in healthy vs ulcerative colitis biopsy derived colonoid monolayers. (*B*) Human colonoid-derived monolayer stained with DRA (*green*) and actin (*red*). (*C*) Representative Z-stack confocal images of colonoid-derived monolayers stained with IL-33 (*green*) and actin (*red*) in wild-type vs DRA KO mice. Scale bar, 5 μm.

regulation of IL-33 in colonocytes. Because alarmin cytokines are also elevated as a result of barrier dysfunction and loss of DRA is known to compromise the barrier, this could be one possible mode by which this cytokine is up-regulated. IL-33 can also be up-regulated because of tissue damage; however, our H&E staining did not show any apparent tissue damage in DRA KO mice (data not shown). In future studies, it would be of interest to further assess the mechanisms underlying the direct role of loss of DRA in increase in colonic IL-33 secretion.

Taken together, the present work highlights the critical relevance of the expression of a chloride transporter on colonocytes to maintain mucosal immune cell homeostasis. Loss of DRA results in a compromised barrier and damage to colonocytes. This triggers the release of the alarmin cytokine IL-33 from the nucleus to drive a type 2 immune cell activation. Although several other immune cells were also altered in DRA KO mice, the overwhelming evidence presented here highlights that IL-33 appears to be the key driver of this phenotype. This feature further underlies vast similarities between human UC and DRA KO mice, validating the use of this preclinical model as a vital tool in studying the emerging role of DRA in UC pathogenesis.

Materials and Methods

Mice

Eight- to 10-week-old WT and DRA KO mice were maintained at Jesse Brown Veterans Affairs Medical Center animal facility. All animal studies were approved by the Animal Care Committee at the University of Illinois at Chicago and Jesse Brown Veterans Affairs Medical Center (Chicago, IL). Once genotyped, all mice were maintained on Pedialyte electrolyte solution until use.[40]

Acute Dextran Sulfate Sodium Colitis

For DSS studies, 8- to 10-week-old age-matched male and female WT and DRA KO mice were administered with 2% w/v DSS MW 36,000–50,000 (MP Biomedicals, Solon, OH) in drinking water for 5 days.

Broad Spectrum Antibiotic and Co-housing Studies

Eight- to 10-week-old age- and sex-matched WT and DRA KO mice were administered with a cocktail of broad spectrum antibiotics consisting of ampicillin (1 g/L), vancomycin (500 mg/L), neomycin sulfate (1 g/L), and metronidazole (1 g/L) in drinking water for 7 days as described previously.[41] In co-housing experiments, WT and DRA KO mice were co-housed for 4 weeks, and gut microbial composition was determined as stated previously by us.[5]

Neutralization of IL-33

IL-33 was neutralized by injecting anti-mouse IL-33 (R& D Biosystems) or immunoglobulin G control at a dose of 1 mg/mouse/day via intraperitoneal injection in male and female WT and DRA KO mice for 1 week as described previously.[42] At the end of the study, mice were euthanized, and the colonic LP immune cells were analyzed as described below.

Isolation of Lamina Propria Lymphocytes

Whole ileal (last one third of the small intestine) and whole colonic (with cecum) LPLs were collected from mice after euthanizing by CO_2 gas. Isolation of LP lymphocytes was performed using differential centrifugation with Percoll gradient as described previously.[43,44]

Cell Staining for Flow Cytometry

Cell staining was performed in 1 million cell per panel for $CD4^+$ T cells and $CD127^+$ ILC populations. Cell surface and transcription factor/cytokine staining was conducted using eBioscience reagents (San Diego, CA) according to the manufacturer's protocol. The antibodies for surface markers were incubated per eBioscience protocol in specified buffers at 1:200 ratio, and the antibodies for transcription factors and cytokines were incubated at a ratio of 1:100. Antibodies are listed in Table 1. Cells were passed through a 40- or 70-μm cell strainer (Corning), and samples were run in Attune NxT flow cytometer (Thermo Fisher Scientific, Waltham, MA). The samples were analyzed using FlowJo software (Franklin Lakes, NJ), with specific gating strategies to identify various T-cell and ILC populations and their secreted cytokines.[43]

Preparation and Culture of Intestinal Explants

Colon and ileum were opened longitudinally and washed thoroughly in sterile 1× phosphate-buffered saline supplemented with 2% fetal bovine serum and 1% penicillin/streptomycin. Fat tissue and Peyer's patches were removed. Two segments from colon and ileum of 1 cm in length per mice (n = 4) of WT and DRA KO mice were placed in 12-well culture plates (Corning) containing fresh RPMI 1640 (Life Technologies) supplemented with 10% fetal bovine serum and 1% penicillin/streptomycin and incubated at 37°C for 16 hours. Segments were kept with the luminal surface exposed to the medium. Supernatants were then harvested, centrifuged at 13,000*g*, and stored at −20°C until used.[42]

IL-33 Enzyme-linked Immunosorbent Assay From Explants and Serum

The concentrations of IL-33 were analyzed by enzyme-linked immunosorbent assay (IL-33 Rat/mouse ELISA; R&D Systems) in sera and tissue supernatants according to the manufacturer's instructions. The sensitivity of the assay was $<20\ \mathrm{pg\,mL^{-1}}$.

Human Biopsy Collection

All patient samples were collected according to the approved Institutional Review Board protocol (2020-1368, UIC) at University of Illinois at Chicago hospital. De-identified healthy (uninflamed from a routine biopsy patient) or UC (diagnosed pancolitis) pinch biopsies from the descending colon were collected by the clinician and provided for crypt isolation and subsequent processing for colonoid/colonoid-derived monolayer generation.

Nanostring Analysis

Scraped colonic mucosa from WT and DRA KO mice (n = 3) was used. RNA was extracted from mucosa using the TRIzol (Qiagen, Germantown, MD) and chloroform (Sigma, St Louis, MO) method as per the manufacturer's protocol into RNAse free water. Fifty nanograms of purified extracted RNA from each sample was processed for transcript analysis by NanoString technologies (Seattle, WA) using the Nanostring nCounter Mouse Immunology panel.[45] Once raw data were acquired, they were further analyzed using the nSolver Analysis Software (NanoString Technologies) and ROSALIND online software platform (San Diego, CA), which is compatible for analyzing Nanostring datasets to identify pathway enrichment and differential gene expression (data deposited in GEO GSE207133; https://nam04.safelinks.protection.outlook.com/?url=https%3A%2F%2Fwww.ncbi.nlm.nih.gov%2Fgeo%2Fquery%2Facc.cgi%3Facc%3DGSE207133&data=05%7C01%7Cdjayaw2%40groute.uic.edu%7Ce62b5d811a0d418ef00408da5938fc32%7Ce202cd477a564baa99e3e3b71a7c77dd%7C0%7C0%7C63.

Immunofluorescence Staining

Formalin-fixed, paraffin-embedded distal colonic tissue was sectioned at 5-μm thickness onto glass slides. These tissues were deparaffinized and stained as described earlier.[46] Colonoids and colonoid-derived monolayers were stained as described before.[47] The primary antibodies used were as follows: DCLK1 and P-120, IL-33, and DRA (Table 1). All antibodies were incubated at a ratio of 1:100 in 1% Normal goat serum (NGS) in phosphate-buffered saline overnight at 4°C in a humidified chamber. Next day slides were washed and incubated with fluorescently tagged secondary antibodies or Phalloidin (Invitrogen) at 1:100 in 1% NGS. Then slides were washed and mounted using SlowFade DAPI reagent (Invitrogen). Slides were stored at −20°C until imaged with confocal microscope (Zeiss).

Quantitative Polymerase Chain Reaction Analysis and Western Blotting

Distal colonic mucosal scarping and epithelial fraction was used for RNA extraction and protein lysate preparation;

Table 1. Antibodies Used for FACS Analysis, Immunostaining, Western Blot Analysis, and In Vivo Studies

Company	Catalog number	Antibody description
Thermo	17-7222-82	IL-22 Monoclonal Antibody (IL22JOP), APC, eBioscience
Fisher Scientific	50-162-19	TCR beta, APC-eFluor 780, clone: H57-597, eBioscience
Fisher Scientific (BD)	BDB562892	$\gamma\delta$ T-Cell Receptor Hamster anti-Mouse, Brilliant Violet 421, Clone: GL3, BD
Fisher Scientific (BD)	BDB563151	CD4 Rat anti-Mouse, Brilliant Violet 605, Clone: RM4-5, BD
Thermo	25-7133-82	IL-13 Monoclonal Antibody (eBio13A), PE-Cyanine7, eBioscience
Thermo	45-0441-82	PerCP-Cyanine5.5 Anti-Human/Mouse CD44 (IM7)
Fisher Scientific	BDB552051	CD4 Rat anti-Mouse, APC-Cy7, Clone: GK1.5, BD
Thermo	67-0081-82	CD8a Monoclonal Antibody (53-6.7), Super Bright 702, eBioscience
Thermo	45-0149-42	CD14 Monoclonal Antibody (61D3), PerCP-Cyanine5.5, eBioscience
Thermo	45-0193-82	CD19 Monoclonal Antibody (eBio1D3 (1D3)), PerCP-Cyanine5.5, eBioscience
Thermo	45-0452-82	CD45R (B220) Monoclonal Antibody (RA3-6B2), PerCP-Cyanine5.5, eBioscience
Thermo	46571182	TCR gamma/delta Armenian Hamster anti-Mouse, PerCP-eFluor 710, Clone: eBioGL3 (GL-3, GL3), eBioscience
Thermo	53-7311-82	IFN gamma Monoclonal Antibody (XMG1.2), Alexa Fluor 488, eBioscience
Fisher Scientific	50-112-3698	CD8a Rat anti-Mouse, PerCP-Cyanine5.5, Clone: 53-6.7, eBioscience
Biolegend	506914-BL	Anti-IL-17A Rat Monoclonal Antibody (Alexa Fluor 700) [clone: TC11-18H10.1]
Fisher Scientific (BD)	BDB742893	BV510 Rat Anti-Mouse I-A/I-E
Thermo	14-7321-81	PE TNF alpha Monoclonal Antibody (MP6-XT22), eBioscience
Thermo	53-9966-42	Gata-3 Monoclonal Antibody (TWAJ), Alexa Fluor 488, eBioscience
Thermo	45-0441-82	PerCP-Cyanine5.5 Anti-Human/Mouse CD44 (IM7)
Thermo	17-5773-82	FOXP3 Monoclonal Antibody (FJK-16s), APC, eBioscience
BD Biosciences	560705	Alexa Fluor 700 Hamster Anti-Mouse TCR β Chain Clone H57-597 (RUO)
BD Biosciences	562894	BV421 Mouse Anti-Mouse RORγt Clone Q31-378 (RUO)
Thermo	12-5825-82	T-bet Monoclonal Antibody (eBio4B10 (4B10)), PE, eBioscience
Thermo	45-0031-82	CD3e Monoclonal Antibody (145-2C11), PerCP-Cyanine5.5, eBioscience
Thermo	45-0112-82	CD11b Monoclonal Antibody (M1/70), PerCP-Cyanine5.5, eBioscience
Fisher Scientific (BD)	562959	BV421 Rat Anti-Mouse CD127 Clone SB/199 (RUO)
Thermo	63-5941-82	NK1.1 Monoclonal Antibody (PK136), Super Bright 600, eBioscience
Thermo	67-5893-80	KLRG1 Monoclonal Antibody (2F1), Super Bright 702, eBioscience
Thermo	12-6981-82	ROR gamma (t) Monoclonal Antibody (B2D), PE, eBioscience
Novus	NBP1-75516	IL-33
Invitrogen	PA5-47007	IL-33
Millipore	05-1567	P-120 Catenin
Abcam	ab31704	DCLK1
Research Resource Center UIC and Pocono Rabbit Farm		DRA*
Sigma	G9545	GAPDH
R&D Biosystems	MAB3626	Mouse anti-IL-33
R&D Biosystems	MAB006	Rat IgGA Isotype control

*DRA antibody was raised against the C-terminal amino acid (745–764) sequence: INTNGGLRNRVYEPVETKF of SLC26A3 (accession number: BC025671) at Pocono Rabbit Farms, Canadensis, PA and at UIC Research Resource Center.

quantitative polymerase chain reaction and Western blotting were performed as described previously.[48] One hundred nanograms of RNA and 30–50 mg of protein were used for each analysis. Gene specific primers are listed in Table 2.

Preparation of Colonoids and Colonoid-Derived Monolayers From Human and Mouse Intestines

Colonoids from WT and DRA KO mice were prepared from isolated crypts as described previously.[5] The colonoids were disrupted, and monolayers were prepared on collagen coated 12-well Transwell inserts as described.[49] Differentiation medium was added after 7 days post plating, and the monolayers were allowed to grow for 7 more days until monolayers were fully differentiated.[50,51] Human biopsy derived colonoids were prepared as described before using STEMCELL human IntestiCult medium.[32] Briefly, the biopsies were minced thoroughly and passaged through a 100-μm strainer and centrifuged at 1000 rpm for 10 minutes. The pellet was suspended in Matrigel and plated in 6-

Table 2. Gene Specific Primer Sequences Used for Quantitative Polymerase Chain Reaction Analysis

Gene	Forward 5'-3'	Reverse 5'-3'
m-DCLK1	CTGGGTTAATGATGATGGTCTCC	TCCTGGTTGTTGGTAGTAGTCC
m-IL-25	ACAGGGACTTGAATCGGGTC	TGGTAAAGTGGGACGGAGTTG
m-IL-33	TCCAACTCCAAGATTTCCCCG	CATGCAGTAGACATGGCAGAA
m-IL1RL1	TGACACCTTACAAAACCCGGA	AGGTCTCTCCCATAAATGCACA
m-GAPDH	TGGATTTGGACGCATTGGTC	TTTGCACTGGTACGTGTTGAT

well plates. Medium was changed every third day.[52] These colonoids were passaged, then disrupted, plated onto coated Transwell inserts, and allowed to differentiate into monolayers for additional 7 days.[53]

Statistical Analysis

Data presented are mean ± standard error of mean of independent observations. One-way analysis of variance was used to compare statistical significance for more than 2 samples and Student t test (two-tailed) for 2 samples. $P < .05$ was considered to be statistically significant.

References

1. Yu Q. Slc26a3 (DRA) in the gut: expression, function, regulation, role in infectious diarrhea and inflammatory bowel disease. Inflamm Bowel Dis 2021;27:575–584.
2. Shao X-x, Lin D-p, Sun L, et al. Association of ulcerative colitis with solute-linked carrier family 26 member A3 gene polymorphisms and its expression in colonic tissues in Chinese patients. Int J Colorectal Dis 2018;33:1169–1172.
3. Asano K, Matsushita T, Umeno J, et al. A genome-wide association study identifies three new susceptibility loci for ulcerative colitis in the Japanese population. Nature Genetics 2009;41:1325.
4. Liu JZ, Van Sommeren S, Huang H, et al. Association analyses identify 38 susceptibility loci for inflammatory bowel disease and highlight shared genetic risk across populations. Nature Genetics 2015;47:979.
5. Kumar A, Priyamvada S, Ge Y, et al. A novel role of SLC26A3 in the maintenance of intestinal epithelial barrier integrity. Gastroenterology 2021;160:1240–1255 e3.
6. Kini A, Singh AK, Riederer B, et al. Slc26a3 deletion alters pH-microclimate, mucin biosynthesis, microbiome composition and increases the TNFα expression in murine colon. Acta Physiologica 2020;230:e13498.
7. Norsa L, Canani RB, Duclaux-Loras R, et al. Inflammatory bowel disease in patients with congenital chloride diarrhoea. J Crohns Colitis 2021.
8. Kere J, Lohi H, Höglund P. Congenital chloride diarrhea. Am J Physiol Gastrointest Liver Physiol 1999;276:G7–G13.
9. Engevik AC, Engevik MA. Exploring the impact of intestinal ion transport on the gut microbiota. Computational and Structural Biotechnology Journal 2021;19:134–144.
10. Furet J-P, Kong L-C, Tap J, et al. Differential adaptation of human gut microbiota to bariatric surgery–induced weight loss: links with metabolic and low-grade inflammation markers. Diabetes 2010;59:3049–3057.
11. Larmonier CB, Laubitz D, Hill FM, et al. Reduced colonic microbial diversity is associated with colitis in NHE3-deficient mice. Am J Physiol Gastrointest Liver Physiol 2013;305:G667–G677.
12. Al-Ghadban S, Kaissi S, Homaidan FR, et al. Cross-talk between intestinal epithelial cells and immune cells in inflammatory bowel disease. Scientific Reports 2016;6:1–13.
13. Bianchi ME. DAMPs, PAMPs and alarmins: all we need to know about danger. J Leukoc Biol 2007;81:1–5.
14. Chatterjee I, Kumar A, Castilla-Madrigal RM, et al. CDX2 upregulates SLC26A3 gene expression in intestinal epithelial cells. Am J Physiol Gastrointest Liver Physiol 2017;313:G256–G264.
15. Griesenauer B, Paczesny S. The ST2/IL-33 axis in immune cells during inflammatory diseases. Frontiers in Immunology 2017;8:475.
16. Pastorelli L, Garg RR, Hoang SB, et al. Epithelial-derived IL-33 and its receptor ST2 are dysregulated in ulcerative colitis and in experimental Th1/Th2 driven enteritis. Proc Natl Acad Sci USA 2010;107:8017–8022.
17. Pastorelli L, De Salvo C, Vecchi M, et al. The role of IL-33 in gut mucosal inflammation. Mediators of Inflammation 2013;2013.
18. Palmieri V, Ebel J-F, Ngo Thi Phuong N, et al. Interleukin-33 signaling exacerbates experimental infectious colitis by enhancing gut permeability and inhibiting protective Th17 immunity. Mucosal Immunology 2021;14:923–936.
19. Roda G, Marocchi M, Sartini A, et al. Cytokine networks in ulcerative colitis. Ulcers 2011;2011.
20. Von Moltke J, Ji M, Liang H-E, et al. Tuft-cell-derived IL-25 regulates an intestinal ILC2–epithelial response circuit. Nature 2016;529:221–225.
21. Wohlfert EA, Grainger JR, Bouladoux N, et al. GATA3 controls Foxp3+ regulatory T cell fate during inflammation in mice. J Clin Invest 2011;121:4503–4515.
22. Phuong NNT, Palmieri V, Adamczyk A, et al. IL-33 drives expansion of type 2 innate lymphoid cells and regulatory T cells and protects mice from severe, acute colitis. Frontiers in Immunology 2021;12.
23. Qiu X, Qi C, Li X, et al. IL-33 deficiency protects mice from DSS-induced experimental colitis by suppressing ILC2 and Th17 cell responses. Inflamm Res 2020;69:1111–1122.
24. Seidelin JB, Bjerrum JT, Coskun M, et al. IL-33 is upregulated in colonocytes of ulcerative colitis. Immunol Lett 2010;128:80–85.
25. Lohi H, Makela S, Pulkkinen K, et al. Upregulation of CFTR expression but not SLC26A3 and SLC9A3 in

ulcerative colitis. Am J Physiol Gastrointest Liver Physiol 2002;283:G567–G575.
26. Xu L, Xiao F, He J, et al. Lysophosphatidic acid increases SLC26A3 expression in inflamed intestine and reduces diarrheal severity in C57BL/6 mice with dextran-sodium-sulfate-induced colitis. Chin Med J 2014;127:1737–1743.
27. Singh V, Kumar A, Raheja G, et al. Lactobacillus acidophilus attenuates downregulation of DRA function and expression in inflammatory models. Am J Physiol Gastrointest Liver Physiol 2014;307:G623–G631.
28. Kini A, Zhao B, Basic M, et al. Upregulation of antimicrobial peptide expression in slc26a3-/-mice with colonic dysbiosis and barrier defect. Gut Microbes 2022;14:2041943.
29. Geremia A, Arancibia-Cárcamo CV. Innate lymphoid cells in intestinal inflammation. Frontiers in Immunology 2017;8:1296.
30. Goldberg R, Prescott N, Lord GM, et al. The unusual suspects: innate lymphoid cells as novel therapeutic targets in IBD. Nature Reviews Gastroenterology & Hepatology 2015;12:271–283.
31. Schulz-Kuhnt A, Neurath MF, Wirtz S, et al. Innate lymphoid cells as regulators of epithelial integrity: therapeutic implications for inflammatory bowel diseases. Frontiers in Medicine 2021;8:656745.
32. Penny HA, Hodge SH, Hepworth MR. Orchestration of intestinal homeostasis and tolerance by group 3 innate lymphoid cells. Semin Immunopathol 2018;40:357–370.
33. Gronke K, Diefenbach A. Tuft cell-derived IL-25 activates and maintains ILC2. Immunol Cell Biol 2016;94:221.
34. Gerbe F, Sidot E, Smyth DJ, et al. Intestinal epithelial tuft cells initiate type 2 mucosal immunity to helminth parasites. Nature 2016;529:226–230.
35. Pastille E, Wasmer M-H, Adamczyk A, et al. The IL-33/ST2 pathway shapes the regulatory T cell phenotype to promote intestinal cancer. Mucosal Immunology 2019;12:990–1003.
36. Meinicke H, Bremser A, Brack M, et al. Tumour-associated changes in intestinal epithelial cells cause local accumulation of KLRG 1+ GATA 3+ regulatory T cells in mice. Immunology 2017;152:74–88.
37. Ohnmacht C, Park J-H, Cording S, et al. The microbiota regulates type 2 immunity through RORγt+ T cells. Science 2015;349:989–993.
38. Britton GJ, Contijoch EJ, Mogno I, et al. Microbiotas from humans with inflammatory bowel disease alter the balance of gut Th17 and RORγt+ regulatory T cells and exacerbate colitis in mice. Immunity 2019;50:212–224 e4.
39. Braun H, Afonina IS, Mueller C, et al. Dichotomous function of IL-33 in health and disease: from biology to clinical implications. Biochem Pharmacol 2018;148:238–252.
40. Walker NM, Simpson JE, Yen PF, et al. Down-regulated in adenoma Cl/HCO3 exchanger couples with Na/H exchanger 3 for NaCl absorption in murine small intestine. Gastroenterology 2008;135:1645–1653 e3.
41. Kiyohara H, Sujino T, Teratani T, et al. Toll-like receptor 7 agonist–induced dermatitis causes severe dextran sulfate sodium colitis by altering the gut microbiome and immune cells. Cell Mol Gastroenterol Hepatol 2019;7:135–156.
42. Guabiraba R, Besnard A-G, Menezes GB, et al. IL-33 targeting attenuates intestinal mucositis and enhances effective tumor chemotherapy in mice. Mucosal Immunology 2014;7:1079–1093.
43. Sano T, Kageyama T, Fang V, et al. Redundant cytokine requirement for intestinal microbiota-induced Th17 cell differentiation in draining lymph nodes. Cell Reports 2021;36:109608.
44. Sano T, Huang W, Hall JA, et al. An IL-23R/IL-22 circuit regulates epithelial serum amyloid A to promote local effector Th17 responses. Cell 2015;163:381–393.
45. Tankou SK, Regev K, Healy BC, et al. A probiotic modulates the microbiome and immunity in multiple sclerosis. Ann Neurol 2018;83:1147–1161.
46. Jayawardena D, Guzman G, Gill RK, et al. Expression and localization of VPAC1, the major receptor of vasoactive intestinal peptide along the length of the intestine. Am J Physiol Gastrointest Liver Physiol 2017;313:G16–G25.
47. Kumar A, Chatterjee I, Anbazhagan AN, et al. Cryptosporidium parvum disrupts intestinal epithelial barrier function via altering expression of key tight junction and adherens junction proteins. Cell Microbiol 2018;20:e12830.
48. Jayawardena D, Anbazhagan AN, Guzman G, et al. Vasoactive intestinal peptide nanomedicine for the management of inflammatory bowel disease. Molecular Pharmaceutics 2017;14:3698–3708.
49. Thorne CA, Chen IW, Sanman LE, et al. Enteroid monolayers reveal an autonomous WNT and BMP circuit controlling intestinal epithelial growth and organization. Dev Cell 2018;44:624–633 e4.
50. Yin J, Tse C-M, Avula LR, et al. Molecular basis and differentiation-associated alterations of anion secretion in human duodenal enteroid monolayers. Cell Mol Gastroenterol Hepatol 2018;5:591–609.
51. Wang Y, Kim R, Gunasekara DB, et al. Formation of human colonic crypt array by application of chemical gradients across a shaped epithelial monolayer. Cell Mol Gastroenterol Hepatol 2018;5:113–130.
52. Mahe MM, Sundaram N, Watson CL, et al. Establishment of human epithelial enteroids and colonoids from whole tissue and biopsy. Journal of Visualized Experiments 2015:e52483.
53. In JG, Foulke-Abel J, Clarke E, et al. Human colonoid monolayers to study interactions between pathogens, commensals, and host intestinal epithelium. Journal of Visualized Experiments 2019:e59357.

Received July 7, 2022. Accepted December 9, 2022.

Correspondence
Address correspondence to: Pradeep K. Dudeja, PhD, University of Illinois at Chicago, Jesse Brown VA Medical Center, Medical Research Service (600/151), 820 South Damen Avenue, Chicago, Illinois 60612. e-mail: pkdudeja@uic.edu.

CRediT Authorship Contributions

Dulari Jayawardena, BPharm, PhD (Conceptualization: Lead; Data curation: Lead; Formal analysis: Lead; Investigation: Lead; Software: Lead; Writing – original draft: Lead; Writing – review & editing: Lead)

Shubha Priyamvada, PhD (Investigation: Supporting; Writing – review & editing: Supporting)

Takahiro Kageyama, MD, PhD (Data curation: Equal; Formal analysis: Equal)

Zachary White, MS (Data curation: Equal; Investigation: Equal; Writing – review & editing: Supporting)

Anoop Kumar, PhD (Funding acquisition: Supporting; Investigation: Supporting)

Theodor Frank Griggs, MD, PhD (Data curation: Supporting; Investigation: Supporting; Writing – review & editing: Supporting)

Apurba Majumdar, MS (Data curation: Supporting)

Ramsha Akram, BS (Data curation: Supporting; Investigation: Supporting)

Arivarasu Natarajan Anbazhagan, PhD (Data curation: Supporting)

Teruyuki Sano, PhD (Conceptualization: Equal; Data curation: Equal; Formal analysis: Equal; Funding acquisition: Equal; Resources: Supporting; Writing – review & editing: Equal)

Pradeep K. Dudeja, PhD (Conceptualization: Supporting; Funding acquisition: Lead; Resources: Equal; Supervision: Equal; Writing – review & editing: Lead)

Conflicts of interest

The authors disclose no conflicts.

Funding

Supported by Department of Veterans Affairs, Veterans Heath Administration, Office of Research and Development, Biomedical Laboratory Research and Development: Merit Review Award: BX002011 (PKD), VA Senior Research Career Scientist Award, 1IK6BX005242 (PKD), and VA CDA2 Award BX004719 (AK). Also supported by NIH/NIDDK grants R01 DK 54016 and DK92441 (PKD) and UIC startup funds (TS).